Optimized Operation of Hybrid Wind-Hydrogen System to Provide Flexibility for Transmission System Needs

Hosna Khajeh, Sahar Seyyedeh-Barhagh, *Student Member, IEEE*, and Hannu Laaksonen, *Member, IEEE*

***Abstract*—This paper focuses on the optimized and coordinated operation of a hybrid system comprising wind turbines, a hydrogen electrolyzer, and hydrogen storage. A day-ahead optimized schedule is developed for the hybrid wind-hydrogen system to provide flexibility in meeting the transmission system operator's needs, offering frequency control support through frequency containment reserves (FCR) and managing congestion on nearby transmission lines. The proposed operation strategy enables effective participation in three reserve markets (FCR-N, upward, and downward FCR-D) while robustly managing uncertainties in wind power forecasting by leveraging the flexibility of the hydrogen electrolyzer and hydrogen storage. Utilizing historical data on FCR activation during normal grid operation and disturbances, this strategy robustly addresses frequency-driven uncertainties. The effectiveness of the proposed method is demonstrated through two case studies using real-world data on frequency deviations and market prices in Finland. Additionally, the proposed strategy is compared with two alternative approaches: one based on spot market prices and another prioritizing self-sufficiency over financial gains.**

***Index Terms*—TSO, hydrogen electrolyzer, FCR, hydrogen storage, reserve markets.**

NOMENCLATURE

• *Abbreviations*

FCR-D	Frequency Containment Reserve for Disturbances.
FCR-N	Frequency Containment Reserve for Normal operations.
HSEW	A hybrid system that includes Hydrogen Storage, Electrolyzer, Wind.
NN	Non Negative variable.
TSO	Transmission System Operator.

• *Sets*

c	Scenario pertaining to either upward or downward activation $\in \{1, 2\}$
d	Time (day) $\in \mathcal{D}$
m	Time (minute) $\in \mathcal{M}$
n, n'	Nodes $\in \mathcal{N}$
r	Segment in piece-wise linearization $\in \mathcal{R}$
s	Scenario associated with wind power forecasts $\in \mathcal{S}$
t	Market timeslot $\in \tau$

• *Variables*

$\theta_{n,t,c}$	Voltage angle at node n and time t for scenario c
$A^{-N,up/down,\max}_{n=HSEW,t,c}$	Maximum activation of FCR-N in upward/downward direction at t and HSEW node for scenario c (NN)
$A^{-D,up/down,\max}_{n=HSEW,t,c}$	Maximum activation of upward/downward FCR-D at t and HSEW node for scenario c (NN)
H^{pro}_t	Hydrogen produced at t (NN)
H^{dir}_t	Hydrogen going directly to demand at t, without storing in the storage (NN)
$H^{in,sto}_t$	Hydrogen injected into the storage at t (NN)
$H^{out,sto}_t$	Hydrogen extracted from the storage at t (NN)
H^{demand}_t	Hydrogen delivered to the demand at t (NN)
SOC^{sto}_t	State of charge of the storage at t (NN)
P^{e}_t	Power consumed by electrolyzer at t (NN)
$P^{e}_{r,t}$	Power consumed by electrolyzer in segment r at t (NN)
P^{-N}_t	FCR-N capacity offered by the HSEW at t (NN)
$P^{-D,up/down}_t$	Upward/downward FCR-D capacity offered by the HSEW at t (NN)
$P^{2grid}_{n=n_0,t,c}$	Power coming to the grid from slack node (n_0) at t for scenario c
P^{com}_t	Power consumed by the compressor at t (NN)
$u^{ON/OFF}_t$	Binary variable indicating whether the electrolyzer is ON/OFF at t
u^{sb}_t	Binary variable indicating whether the electrolyzer is in the standby state at t
u^{su}_t	Binary variable indicating whether the electrolyzer starts up at t
$u_{r,t}$	Binary variable indicating whether segment r is active at t

Received 8 August 2024; revised 8 November 2024; accepted 16 December 2024. Date of publication 18 December 2024; date of current version 23 June 2025. This work was supported in part by the Smart Grid 2.0 Project (Next Generation Distribution Grid) funded by Business Finland under Grant 1386/31/2022 and in part by Finnish Companies. Paper no. TSTE-00999-2024. *(Corresponding author: Hannu Laaksonen.)*

The authors are with the Flexible Energy Resources Team, School of Technology and Innovations, University of Vaasa, 65100 Vaasa, Finland (e-mail: hannu.laaksonen@uwasa.fi).

Color versions of one or more figures in this article are available at https://doi.org/10.1109/TSTE.2024.3519953.

Digital Object Identifier 10.1109/TSTE.2024.3519953

• *Parameters*

α_r, β_r	Parameters associated with hydrogen's piece-wise linearization.
π_t^{-N}	Price of reserving FCR-N capacity at t
$\pi_t^{-D,up/down}$	Price of reserving upward/downward FCR-D capacity at t
π^H	Hydrogen price.
$\pi_t^{reg,up/down}$	Up/down regulation price at t
π^{su}	startup cost of electrolyzer.
$\theta^{\min\,/\,\max}$	Minimum/maximum voltage angle allowed.
$\overline{\Delta f_t^{-N,up/down}}$	Average frequency deviation associated with upward/downward activation of FCR-N at t
$\overline{\Delta f_t^{-D,up/down}}$	Average frequency deviation associated with upward/downward activation of FCR-D at t
$\widehat{\Delta f_t^{-N,up/down}}$	Maximum of frequency deviation average associated with upward/downward activation of FCR-N at t
$\widehat{\Delta f_t^{-D,up/down}}$	Maximum of frequency deviation average associated with upward/downward activation of FCR-D at t
$\overline{\Delta P_t^w}$	Average error regarding wind power forecast scenarios.
$B_{n,n'}$	Susceptance of the line between nodes n and n'
$\widehat{SOC^{sto}}$	Maximum state of charge of hydrogen storage.
$\widehat{D^H}$	Maximum hydrogen demand that should be delivered throughout a day.
$f_{t,m}$	Frequency measured at minute m and market timeslot t
$\widehat{H^{out,sto}}$	Maximum hydrogen that can be extracted from the storage.
K^c	Compression coefficient.
Pf-droop	Active Power frequency-droop.
$P_{n,t}^p$	Power produced at t and node n
$P_{n,t}^d$	Power consumed at t and node n
$P_t^{\text{wind},\min\,/\,\max}$	Minimum/maximum forecasted wind power at t
$P^{e,\min\,/\,\max}$	Minimum/maximum power that can be consumed by the electrolyzer.
$P_{n,n'}^{e,\min\,/\,\max}$	Minimum/maximum power that can flow between nodes n and n'
P^{sb}	Power consumed by the electrolyzer in its standby mode.

I. Introduction

EUROPE aims to lead in hydrogen production and infrastructure development, aligning with the EU Green Deal's goal of accelerating renewable energy construction, with a particular emphasis on green hydrogen [1]. This involves doubling hydrogen valleys across Europe [1]. However, integrating large-scale electrolyzers poses challenges for both local transmission grids and broader energy systems [1]. These challenges include disrupting system balance and causing network congestion. Therefore, effective coordination between hydrogen production and energy systems is crucial to enable the electrical grid to accommodate the widespread integration of hydrogen.

Some studies conclude that the flexible and optimized operation of hydrogen systems could, in turn, decrease electricity prices and reduce renewable curtailments. For example, Reference [2] argued that the flexible operation of hydrogen can stabilize the price of renewable energy in future renewable-based power systems. The study conducted by [3] indicated that an increase in hydrogen demand by deploying more hydrogen fuel cell electric vehicles could not only support effective grid operation but also lower electricity costs. The authors of [4] discussed that the utilization of hydrogen as a fuel for heating residential houses can affect energy prices and lower renewable generation curtailment. Ref. [5] analyzed the positive impacts of the hydrogen system on market clearing results and the hydrogen system's role in electricity prices. Finally, Reference [6] concluded that the hybrid system of hydrogen and renewable energy systems led to up to 30% cost savings.

Besides optimization based on electricity prices, another economically efficient coordination solution is to use hydrogen systems to offer ancillary services to power system operators. In this regard, some research analyzed the technical feasibility of providing ancillary services by hydrogen systems. For example, Reference [7] focused on the technical aspects of Proton Exchange Membrane (PEM) electrolyzer technologies, analyzing their eligibility to comply with the requirements of European ancillary services markets. Reference [8] analyzed the technical potential of the alkaline electrolyzer plant when it provides dynamic frequency regulation service to the TSO. In another work, Reference [9] reviewed the papers proposing the flexible operation of electrolyzers and discussed that hydrogen electrolyzers' capabilities to provide ancillary services. The research conducted by [10] assessed the dynamic characteristics and potential of the electrolyzer's stack for frequency regulation for a power system dominated by solar photovoltaic units. Reference [11] investigated the provision of fast frequency reserve by electrolyzers in low inertia situations. The paper gave special emphasis to the nonlinearity of modeling the electrolyzer and the impacts on its service provision. In Reference [12], authors conducted extended research on a dynamic model of the electrolyzer interfaced with power electronics equipment that provides fast frequency services for the TSO. Reference [13] proposed a method to aggregate electrolyzers with VPP that provides voltage control services to the local distribution system operator. Similarly, an accurate real-time simulation model for hydrogen production in response to frequency deviations was developed in [14], ensuring contractual compliance while improving system frequency regulation. Advanced control strategies have been implemented to enhance the cost-efficiency and responsiveness of hydrogen systems; however, the model was not specifically designed for any particular flexibility service. Additionally, a dynamic model incorporating both PEM and

TABLE I
COMPARISON OF THE MAIN FACTORS CONSIDERED IN THE LITERATURE WITH THOSE IN THIS PAPER

Reference	Hydrogen system	Service provided	Uncertainty of renewables	Uncertainty of activation
[16]	Electrolyzer, compressor, storage, fuel cell	Balancing service	No	Not exactly
[17]	Photovoltaic system, storage, electrolyzer	Regulation service	Yes	Not robustly
[18]	Hybrid electrolyzers	Frequency regulation service	No	No
[19]	Electrolyzer, compressor, storage, fuel cell	Secondary frequency reserve	No	No
[15]	Electrolyzer	Virtual inertia, frequency reserves	No	No
[20]	Electrolyzer	Balancing service	Yes	No
[21]	Electrolyzer, compressor, storage	Secondary frequency reserve	Yes	No
[22]	Electrolyzer	FCR-N, FCR-D	No	No
This paper	Electrolyzer, compressor, storage	FCR-N, FCR-D, network-related service	Yes	Yes

alkaline electrolyzer technologies demonstrated the ability of hydrogen systems to provide Frequency Control Ancillary Services in [15], including virtual inertia and primary frequency response, thereby contributing to grid stability. The model involves real-time control of the electrolyzers and their response to grid flexibility requirements, without the need to robustly consider uncertainties.

In addition to technical aspects, limited research has been done to focus on estimating the flexible capacity of hydrogen systems to participate in ancillary service markets complying with the requirements of the specific ancillary service. For example, Reference [16] conducted a long-term profitability analysis by developing a mathematical model of a PV producer integrated with battery storage and a hydrogen system participating in the multi-energy markets as well as balancing markets. The work utilized the general "balancing service" term and did not specify the type of balancing service. However, each frequency regulation service defined in a specific area has its own technical requirements and market characteristics. A chance-constrained stochastic model was proposed in [17] for a hybrid PV-BESS-Electrolyzer system, demonstrating the benefits of balancing hydrogen production with ancillary grid services. Although this approach attempts to model uncertainty in renewable generation and in the energy content of the frequency regulation signal, it does not robustly account for the effects of these uncertainties on the operation of the hybrid system. In real-world applications, the penalty cost of failing to react to frequency deviations can be considerably high. In another study, a decentralized dynamic power-sharing approach for hybrid hydrogen electrolyzer systems was proposed in [18] to efficiently manage frequency deviations. This approach utilized fast-response PEM electrolyzers and cost-effective alkaline electrolyzers for large-scale applications. However, the model lacks optimization, as no mathematical optimization was employed, and uncertainties were disregarded in the research.

Authors of [19] developed an optimization-based approach for a system consisting of PV and hydrogen systems based on the concept of power-to-power trading. It also provides secondary frequency control service for TSO. Results showed that participation in the day-ahead and ancillary service markets can be financially viable and beneficial, particularly when markets exhibit significant price volatility. In another work, Reference [15] modeled hydrogen electrolyzers that provide frequency control services, including virtual inertia as well as primary and secondary frequency response with a focus on Australian ancillary service markets. Reference [20] examined how electrolyzers can support the operation of an energy island when combined with offshore wind energy. In [21], authors presented a method for a wind-electrolysis joint system to provide secondary frequency regulation aiming to reduce the production cost of green hydrogen. This flexibility provision does not consider the network and also did not model the real-time activation impacts on the system's operation.To the best of authors' knowledge, [22] is the only research that suggests using an electrolyzer for FCR provision. However, the authors did not consider the impact of frequency-driven reserve activation on the electrolyzer's operation and the electrolyzer's effects on the transmission grid.

Table I compares the literature in terms of the hydrogen system analyzed, the type of ancillary service proposed, and whether a model was proposed to handle uncertainties of renewables integrated with the hydrogen system, as well as uncertainties associated with frequency-driven service activation. The final row highlights this paper, showcasing its unique features that distinguish it from the others.

In most ancillary service markets, participants estimate their flexible capacity one day in advance. To accurately estimate their flexible capacity, hydrogen systems need to consider different service activation scenarios, which can significantly affect their revenue. This challenge is heightened when hydrogen systems are integrated with renewable energy sources like wind, due to the inherent unpredictability of renewable energy forecasts. Despite this, current literature does not offer a comprehensive method for addressing all key uncertainties involved in estimating the flexible operation of hydrogen systems. To address the gap, this paper proposes an optimization approach to coordinate the operations of a hydrogen storage, electrolyzer, and wind (HSEW) system. The goal is to provide flexibility services to the transmission system operator (TSO). The flexibility services studied include frequency control support through FCR markets and participation in congestion management for transmission lines near the HSEW system. Additionally, the study adopts the piecewise three-state model of an alkaline electrolyzer to account for the non-linear behavior of the hydrogen system. The primary contributions of this paper are as follows:

- This paper examines the HSEW system's participation in three reserve markets (FCR-N, upward and downward FCR-D) while simultaneously managing congestion in the nearby transmission network. The technical and market requirements of these services are all modeled and considered in this paper.

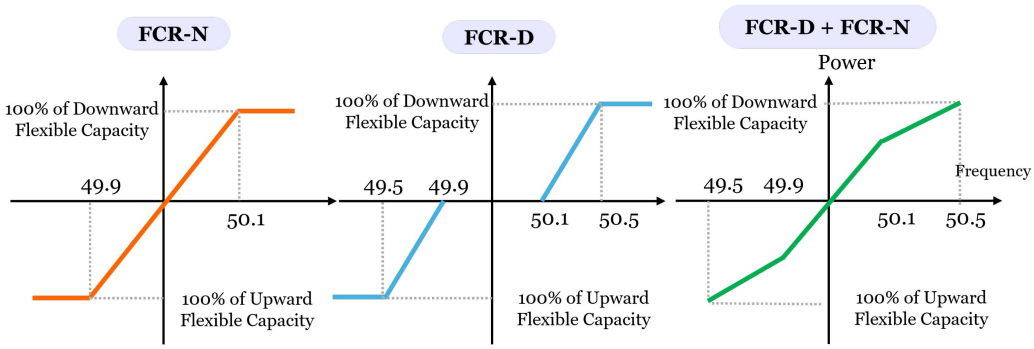

Fig. 1. Illustration of Pf droop profiles for providing FCR services.

- It proposes a novel robust approach to handle two key uncertainties in day-ahead flexible capacity estimation:
  - Frequency-driven FCR activations: By modeling worst-case scenarios for both maximum upward and downward activations, the approach ensures the HSEW can maintain network stability under extreme frequency deviations.
  - Wind power forecasts: To address wind forecast uncertainties, the model considers minimum wind scenarios for upward capacity and maximum wind scenarios for downward capacity, ensuring the HSEW can balance power needs effectively.

Furthermore, the paper develops two other strategies, named Spot and Self-sufficiency strategies, which operate under different frameworks. The paper compares hydrogen production, operation, and profitability of the HSEW in the proposed model with these two strategies using real-world market data from Finland.

The rest of the paper is organized as follows: Section II describes the characteristics of the FCR services including the payment and market participation. Section III develops the optimization problem regarding the coordinated operation of the HSEW. The case studies are introduced in Sections IV and V and the results are visualized and discussed in Sections IV-A and V-A. Finally, Section VI concludes the paper.

II. FCR Provision

FCR providers competitively submit bids on a daily basis to provide FCR, allowing the TSO to secure its required flexible capacity strategically. In real-time, these frequency control support providers must adjust their power generation or consumption to match grid frequency deviations, aligning with their accepted capacity reservations. Fig. 1 demonstrates how providers modify their active power generation or consumption, precisely matched to their allocated capacity, in response to observed frequency changes [23].

FCR markets consist of three primary products: FCR-N, upward FCR-D, and downward FCR-D. These products are designed to respond to specific frequency deviations and ensure grid stability. FCR-N is a symmetric product that can adjust power output in both upward and downward directions. It is typically activated when the frequency deviates 0.1 Hz from the nominal value of 50 Hz. Upward FCR-D providers act as disturbance responders when the frequency deviation is between 49.1 and 49.5 Hz. They inject more power into the grid (decrease consumption or increase production) to bring the frequency back up. Downward FCR-D providers step in to restrain frequency increases that surpass from 50.1 up to 50.5 Hz. Downward flexibility products consume more power by increasing consumption or decreasing production to reduce frequency.

The droop settings for FCR-N and FCR-D are designed to maintain effective frequency regulation within the power system, responding to frequency deviations around the nominal 50 Hz. FCR-N, with a sensitive droop setting of 0.1, operates within a narrow frequency range (49.9 Hz to 50.1 Hz) to ensure stability during normal conditions. In contrast, FCR-D, with a less sensitive droop setting of 0.4, manages larger deviations (49.9 Hz to 49.5 Hz upwards and 50.1 Hz to 50.5 Hz downwards) to handle significant disturbances without overreacting. These settings balance system stability with the technical capabilities of power units, enabling precise control in stable conditions and robust response during disruptions.

Alkaline electrolysis stacks typically use modular power supplies, such as DC switching power supplies, which can be configured in series or parallel to meet specific power requirements. This modular design allows individual cell stacks to be quickly activated or deactivated as power demands change [24]. Additionally, recent studies indicate that advancements in alkaline electrolyzer technology enable ramp rates of up to 20% of nominal load per second, with response times of only a few seconds, demonstrating that alkaline electrolyzers are well-suited for providing FCR services [25].

If an HSEW participates in the FCR-N and FCR-D markets, it must submit its planned capacity allocations for each service one day in advance. The HSEW first determines the flexibility it can offer to the FCR-N and FCR-D capacity markets (Flexible Capacities in Fig. 2), aiming to maximize its profit while ensuring operational and market requirement constraints are met. The paper focuses on robustly determining the hourly capacity available for each service. Once the HSEW submits its capacity availability, the TSO clears the capacity markets and communicates the accepted capacities to the HSEW. In real-time, the HSEW then responds to frequency

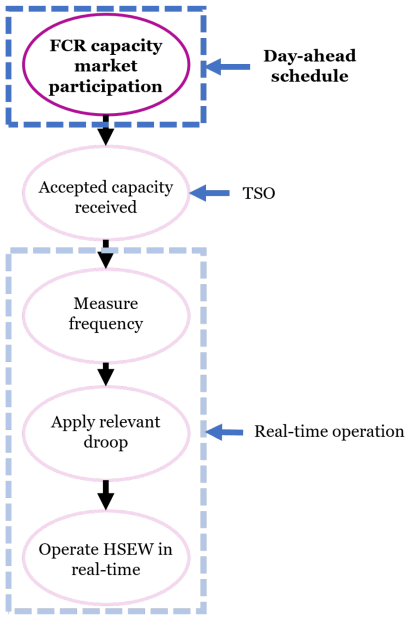

Fig. 2. Illustration of the steps undertaken by the HSEW to provide FCR services, with the scope of this paper highlighted in darker color.

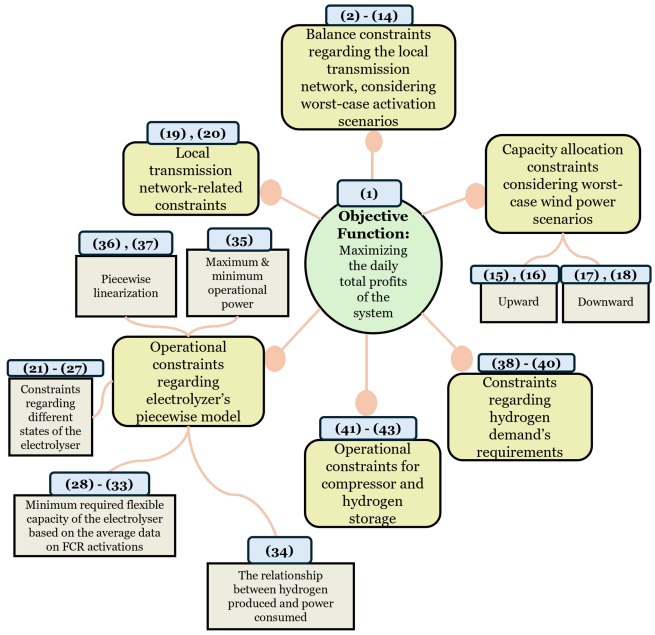

Fig. 3. Summary of the objective function and constraints used in the problem formulation.

deviations based on the droop control for each market and the accepted flexible capacities. Fig. 1 provides an illustration of this process, with the lighter-colored areas indicating aspects beyond the scope of this paper. In our proposed bidding strategy, the HSEW assumes a conservative approach, planning as if 100% of the capacity will be accepted by the TSO. Additionally, the paper presents a robust method for incorporating the effects of real-time activation and potential frequency deviations into the day-ahead bidding strategy.

If the HSEW provides FCR-N, it earns revenue based on the price of the FCR-N capacity market. Additionally, it receives revenue in line with the up-regulation price when the FCR-N activates in the upward direction [26]. However, the HSEW incurs a payment if the FCR-N capacity activates in the downward direction, in accordance with the down-regulation price [26], [27]. On the other hand, FCR-D services do not entail energy remuneration. The HSEW only receives revenue by reserving its capacity for FCR-D, and no payment is transacted in either activation direction [27].

In this paper, HSEW is daily scheduled to provide FCR services, including FCR-N, upward FCR-D, and downward FCR-D. When the grid frequency drops below 50 Hz, the HSEW injects wind power into the grid. To counteract frequency increases above 50 Hz, the HSEW increases the power consumption of electrolyzer. Moreover, we assume a fixed-term contract between the TSO and the HSEW so that the HSEW prevents congestion in the local transmission grid.

III. Problem Formulation

Fig. 3 summarizes equations (1)-(43) used in the optimization model for the optimal day-ahead scheduling of the HSEW. The objective function maximizes the HSEW's revenue from providing FCR services and selling hydrogen:

$$\max_{P_t^{-N},P_t^{-D,up},P_t^{-D,down}} \sum_{t\in\tau} \overbrace{H_t^{demand}\pi^H}^{\text{Hydrogen Selling Revenue}} + \underbrace{P_t^{-N}\pi_t^{-N} + P_t^{-D,up}\pi_t^{-D,up} + P_t^{-D,down}\pi_t^{-D,down}}_{\text{Capacity Revenue}} + \underbrace{\overline{\Delta f_t^{-N,up}} P_t^{-N}\pi_t^{reg,up}}_{\text{Activation Revenue}} - \underbrace{\overline{\Delta f_t^{-N,down}} P_t^{-N}\pi_t^{reg,down}}_{\text{Activation Cost}} - \underbrace{\pi^{su}u_t^{su}}_{\text{Startup Cost}} \tag{1}$$

Where, Hydrogen Selling Revenue indicates the revenue from selling hydrogen at the fixed price π^H. Capacity Revenue comprises the revenues earned by reserving capacity for FCR-N, upward FCR-D and downward FCR-D. If FCR-N capacity is activated upward, the HSEW receives Activation Revenue according to up-regulation prices. Conversely, if FCR-N activates downward, the HSEW incurs the Activation Cost based on down-regulation prices. The last term in (1) refers to the cold startup cost of the electrolyzer, which is incurred during each startup. This startup cost accounts for electrode wear and catalyst degradation associated with the cold start of the electrolyzer.

The introduced objective function is subjected to the constraints that explain the HSEW's operational limits as well as FCR services' requirements. Besides offering FCR services, the HSEW also provides the TSO with network congestion management services, ensuring that network constraints are upheld even in the worst-case FCR activations. In this context, the equation

of power balance for each node is considered a constraint and expressed as follows:

$$\begin{aligned} &A^{-N,up,\max}_{n=HSEW,t,c} - A^{-N,down,\max}_{n=HSEW,t,c} + A^{-D,up,\max}_{n=HSEW,t,c} \\ &- A^{-D,down,\max}_{n=HSEW,t,c} + P^{2grid}_{n=n_0,t,c} - P^{d}_{n,t} + P^{p}_{n,t} \\ &= \sum_{n' \in \mathcal{N}-n} B_{n,n'}(\theta_{n,t,c} - \theta_{n',t,c}) \\ &\forall n' \in \mathcal{N}, \forall t \in \tau, \forall c \in \{1,2\} \end{aligned} \tag{2}$$

In the power balance equation, the worst-case activation of upward FCRs is represented with a positive sign, while the activation of downward FCRs is denoted with a negative sign. This convention reflects that upward flexibility contributes to increased production, while downward flexibility corresponds to increased consumption.

In the first worst-case activation scenario ($c = 1$), the TSO activates only downward for both FCR-N and FCR-D capacities throughout the entire timeslot, meaning that threre is no upward activations:

$$A^{-N,up,\max}_{n=HSEW,t,c=1} = 0 \quad \forall t \in \tau \tag{3}$$

$$A^{-D,up,\max}_{n=HSEW,t,c=1} = 0 \quad \forall t \in \tau \tag{4}$$

$$A^{-N,down,\max}_{n=HSEW,t,c=1} = \frac{\Delta \widehat{f_t^{-N,down}}}{0.1} P_t^{-N} \quad \forall t \in \tau \tag{5}$$

$$A^{-D,down,\max}_{n=HSEW,t,c=1} = \frac{\Delta \widehat{f_t^{-D,down}}}{0.4} P_t^{-D,down} \quad \forall t \in \tau \tag{6}$$

In (5) and (6), the values 0.1 and 0.4 are based on Pf droop settings, as illustrated in Fig. 1, and are specific to the determination of FCR-N and FCR-D services. In this paper, we calculate the maximum average frequency deviations as follows:

$$\Delta \widehat{f_t^{-D,down}} = \max_{d \in \mathcal{D}} \mathcal{R}^{-D\downarrow} = \max_{d \in \mathcal{D}} \begin{cases} \frac{1}{N_m} \sum_m (f_{d,t,m} - 50.1), \\ \text{if } 50.1 \le f_{d,t,m} \le 50.5 \\ 0.4, \text{ if } f_{d,t,m} \ge 50.5. \\ \\ 0 \text{ otherwise.} \end{cases} \tag{7}$$

$$\Delta \widehat{f_t^{-N,down}} = \max_{d \in \mathcal{D}} \mathcal{R}^{-N\downarrow} = \max_{d \in \mathcal{D}} \begin{cases} \frac{1}{N_m} \sum_m (f_{d,t,m} - 50), \\ \text{if } 50 \le f_{d,t,m} \le 50.1 \\ 0.1, \text{ if } f_{d,t,m} \ge 50.1. \\ \\ 0 \text{ otherwise.} \end{cases} \tag{8}$$

Where $\mathcal{R}^{-N\downarrow}$ and $\mathcal{R}^{-D\downarrow}$ indicate the frequency deviation functions for downward FCR-N and FCR-D, obtained from Fig. 1. Equation (7) examines historical events $\mathcal{D}$, find situations where frequencies have surpassed 50.1, and computes the average deviations for downward FCR-D at each timeslot t. It then identifies its maximum frequency deviations as the value of $\Delta \widehat{f_t^{-D,down}}$. In our paper, we adopt a frequency resolution of 1 minute and have analyzed the frequency data over the past year. Correspondingly, (8) calculates maximum of average frequency deviations for downward FCR-N at each timeslot t ($\Delta \widehat{f_t^{-N,down}}$) when frequencies have exceeded 50.

In the second worst-case activation scenario ($c = 2$), only upward activation is requested for both FCRs, with the downward activations set to zero:

$$A^{-N,down,\max}_{n=HSEW,t,c=2} = 0 \quad \forall t \in \tau \tag{9}$$

$$A^{-D,down,\max}_{n=HSEW,t,c=2} = 0 \quad \forall t \in \tau \tag{10}$$

$$A^{-N,up,\max}_{n=HSEW,t,c=1} = \frac{\Delta \widehat{f_t^{-N,up}}}{0.1} P_t^{-N} \quad \forall t \in \tau \tag{11}$$

$$A^{-D,up,\max}_{n=HSEW,t,c=1} = \frac{\Delta \widehat{f_t^{-D,up}}}{0.4} P_t^{-D,up} \quad \forall t \in \tau \tag{12}$$

Where, the calculation of maximum frequency deviations for upward activation of FCRs is computed as follows:

$$\Delta \widehat{f_t^{-D,up}} = \max_{d \in \mathcal{D}} \mathcal{R}^{-D\uparrow} = \max_{d \in \mathcal{D}} \begin{cases} \frac{1}{N_m} \sum_m (49.9 - f_{d,t,m}), \\ \text{if } 49.5 \le f_{d,t,m} \le 49.9. \\ 0.4, \text{ if } f_{d,t,m} \le 49.5. \\ \\ 0 \text{ otherwise.} \end{cases} \tag{13}$$

$$\Delta \widehat{f_t^{-N,up}} = \max_{d \in \mathcal{D}} \mathcal{R}^{-N\uparrow} = \max_{d \in \mathcal{D}} \begin{cases} \frac{1}{N_m} \sum_m (50 - f_{d,t,m}), \\ \text{if } 49.9 \le f_{d,t,m} \le 50. \\ 0.1, \text{ if } f_{d,t,m} \le 49.9 \\ \\ 0 \text{ otherwise.} \end{cases} \tag{14}$$

$\mathcal{R}^{-N\uparrow}$ and $\mathcal{R}^{-D\uparrow}$ indicate the frequency deviation functions for upward FCR-N and FCR-D, obtained from Fig. 1. As (13) and (14) indicate, the maximum frequency deviation for each timeslot is determined by calculating the average frequency deviations over the past year and selecting the maximum deviation value for each timeslot.

It should be noted that the overall schedule (capacities allocated to each FCR service) must remain consistent across both activation scenarios. This means that the optimized day-ahead schedule of the HSEW must be robust enough to handle both extreme cases.

This paper assumes that when upward FCRs are activated, the HSEW injects its wind power into the grid. Conversely, in situations where downward activation is necessary, the electrolyzer increases the consumption of electricity. In the downward situation, although wind power may still be generated, the electrolyzer is configured to absorb wind power to prevent any injection into the grid.

Given that the HSEW scheduling is conducted on a day-ahead basis, wind power is susceptible to forecast errors. Consequently, we have devised various scenarios for wind power and selected the scenario with the minimum wind power as the upper limit for upward capacity to consider the robust scheduling:

$$P_t^{-N} + P_t^{-D,up} \le P_t^{\text{wind,min}} \quad \forall t \in \tau \tag{15}$$

$$P_t^{\text{wind,min}} = \min_{s\in\mathcal{S}} P_{t,s}^{\text{wind}} \quad \forall t \in \tau \tag{16}$$

As expressed in constraint (15), the upward capacity of the HSEW can subsequently be allocated between FCR-N and upward FCR-D. For the downward capacity, to guarantee the provision of downward FCRs, the worst-case scenario is contemplated by anticipating that the electrolyzer should absorb the maximum forecasted wind production:

$$P_t^{-N} + P_t^{-D,down} \leq P^{e,\max} - P_t^{\text{wind,max}} \quad \forall t \in \tau \tag{17}$$

$$P_t^{\text{wind,max}} = \max_{s\in\mathcal{S}} P_{t,s}^{\text{wind}} \quad \forall t \in \tau \tag{18}$$

As indicated in (17), the maximum downward capacity of the HSEW is determined by subtracting the maximum forecasted wind power at time t from the maximum consumption capacity of the electrolyzer. Since FCR-N capacity is symmetric it needs to be considered to both upward and downward capacity constraints i.e. (15) and (17).

The following constraints ensure that the voltage angles of nodes and the limits on line power flow are maintained within their permissible ranges:

$$P_{n,n'}^{\min} \leq B_{n,n'}(\theta_{n,t,c} - \theta_{n',t,c}) \leq P_{n,n'}^{\max}$$
$$\forall t \in \tau, \forall n \in \mathcal{N}, \forall c \in \{1,2\} \tag{19}$$

$$\theta^{\min} \leq \theta_{n,t,c} \leq \theta^{\max} \quad \forall t \in \tau, \forall n \in \mathcal{N}, \forall c \in \{1,2\} \tag{20}$$

This paper adopts the three-state model for alkaline electrolyzers, originally proposed in [28]. At each timeslot, the electrolyzer can operate in only one of three modes: ON (active hydrogen generation), OFF (complete shutdown), or standby (partial power, enabling quick startup):

$$u_t^{ON} + u_t^{OFF} + u_t^{sb} = 1 \quad \forall t \in \tau \tag{21}$$

The power consumption in the ON state must stay within the specified minimum load limit and maximum capacity of the electrolyzer while the standby state has a constant consumption (P^{sb}):

$$P_t^e \leq u_t^{ON} P^{e,\max} + u_t^{sb} P^{sb} \quad \forall t \in \tau \tag{22}$$

$$P_t^e \geq u_t^{ON} P^{e,\min} + u_t^{sb} P^{sb} \quad \forall t \in \tau \tag{23}$$

During each cold startup, the electrolyzer transitions from the OFF (not ON or stand-by) state at $t-1$ to the ON state at t, as modeled by (24):

$$u_t^{su} \geq u_t^{ON} - u_{t-1}^{ON} - u_{t-1}^{sb} \quad \forall t \in \tau \tag{24}$$

However, the electrolyzer cannot come from the OFF to the standby state:

$$u_{t-1}^{OFF} + u_t^{sb} \leq 1 \quad \forall t \in \tau \tag{25}$$

No startup costs are considered during the initial timeslot:

$$u_{t=1}^{su} = 0 \tag{26}$$

This paper suggests introducing a constraint, which was not considered in [28] to ensure that the binary variable representing startup does not equal one when the electrolyzer is not ON:

$$u_t^{ON} \geq u_t^{su} \tag{27}$$

The following constraint estimates the minimum real-time power consumption of the electrolyzer, influenced by both the activation of FCR services and various wind power injection scenarios:

$$P_t^e \geq \overbrace{\frac{\overline{\Delta f_t^{-N,down}}}{0.1} P_t^n + \frac{\overline{\Delta f_t^{-D,down}}}{0.4} P_t^{-D,down}}^{\text{Consumption regarding downward FCRs activation}}$$

$$+ \underbrace{P_t^{-N} + P^{-D,up} - \left(\frac{\overline{\Delta f_t^{-N,up}}}{0.1} P_t^{-N} + \frac{\overline{\Delta f_t^{-D,up}}}{0.4} P_t^{-D,up} \right)}_{\text{Non-activated upward FCRs}}$$

$$+ \overline{\Delta P_t^w} \quad \forall t \in \tau \tag{28}$$

In (28), the terms $\overline{\frac{\Delta f_t^{-N,up/down}}{0.1}}$ and $\overline{\frac{\Delta f_t^{-D,up/down}}{0.4}}$ denote the mean values of activation ratio, which are estimated from the historical activations, as illustrated by (29), (30), (31), and (32):

$$\overline{\Delta f_t^{-D,up}} = \frac{1}{N_D} \mathcal{R}^{-D\uparrow} \tag{29}$$

$$\overline{\Delta f_t^{-D,down}} = \frac{1}{N_D} \mathcal{R}^{-D\downarrow} \tag{30}$$

$$\overline{\Delta f_t^{-N,up}} = \frac{1}{N_D} \mathcal{R}^{-N\uparrow} \tag{31}$$

$$\overline{\Delta f_t^{-N,down}} = \frac{1}{N_D} \mathcal{R}^{-N\downarrow} \tag{32}$$

As per (28), the electrolyzer is designed to consume energy in response to the activation of downward FCRs. Additionally, it is required to absorb the non-activated segment of upward FCRs originating from wind power. Given our consideration of the minimum wind power scenario, the electrolyzer must also account for absorbing the average error in forecasted wind. The error is estimated based on the minimum wind power scenario considered when determining the maximum reserve capacity limit. Estimating this average error involves analyzing different wind scenarios and their respective probabilities:

$$\overline{\Delta P_t^w} = \sum_{s\in\mathcal{S}} \rho_s (P_{t,s}^{\text{wind}} - P_t^{\text{wind,min}}) \quad \forall t \in \tau \tag{33}$$

Where ρ_s refers to the probability of scenario s.

As suggested in [28], the function representing the electrolyzer's hydrogen production in relation to its electricity consumption has been linearized in a piecewise manner to model the non-linear efficiency of the electrolyzer. The resulting function is as follows:

$$H_t^{pro} = \sum_{r\in\mathcal{R}} \alpha_r P_{r,t}^e + \beta_r u_{r,t} \quad \forall t \in \tau \tag{34}$$

Also, each linearized segment needs to remain within its lower and upper bounds:

$$P_{r,t}^{e,\min} u_{r,t} \leq P_{r,t}^e \leq P_{r,t}^{e,\max} u_{r,t} \quad \forall t \in \tau, \forall r \in \mathcal{R} \tag{35}$$

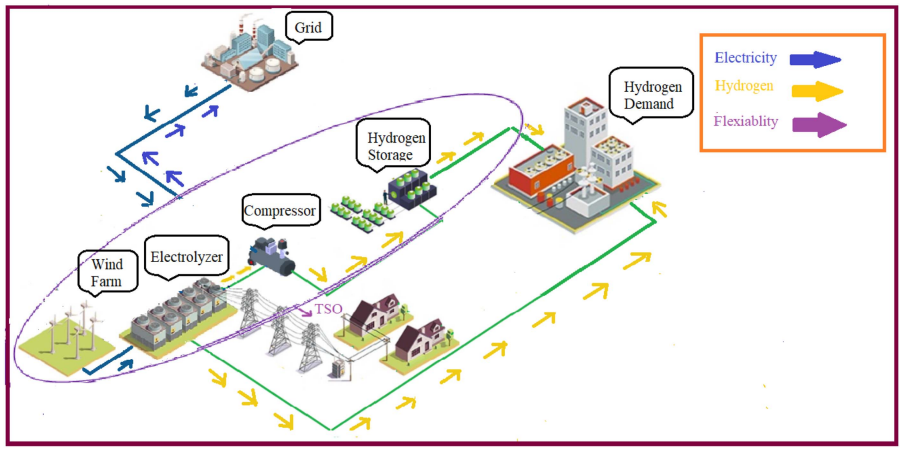

Fig. 4. Illustration of the HSEW providing flexibility services to the TSO while selling hydrogen to the demand.

The electrolyzer in its on-state operates exclusively within the efficiency that is obtained from (36):

$$u_t^{ON} = \sum_{r \in \mathcal{R}} u_{r,t} \quad \forall t \in \tau \tag{36}$$

The following formulation specifies that the electricity consumption of the electrolyzer is determined by the sum of linearized segments when it is ON, and by a constant power when it is in standby mode:

$$P_t^e = \sum_{r \in \mathcal{R}} P_{r,t}^e + u_t^{sb} P^{sb} \quad \forall t \in \tau \tag{37}$$

A portion of the total hydrogen produced by the electrolyzer is immediately routed to meet current demand, while the remainder is stored in the hydrogen storage system, as depicted in Fig. 4. Equation (37) precisely articulates the balance among hydrogen production, its immediate demand, and the amount reserved in the storage:

$$H_t^{pro} = H_t^{dir} + H_t^{in,sto} \quad \forall t \in \tau \tag{38}$$

Additionally, there is another equation that explains how the hydrogen delivered to meet demand can come from storage (as the output of storage) or directly from the electrolyzer. This concept is shown in Fig. 4 and written in math like this:

$$H_t^{demand} = H_t^{dir} + H_t^{out,sto} \quad \forall t \in \tau \tag{39}$$

This paper operates under the assumption of a daily minimum threshold for required hydrogen, as shown in (40). The minimum hydrogen level should be a conservative estimate, providing a buffer for any deviations from ideal conditions.

$$\sum_{t \in \tau} H_t^{demand} \geq \widehat{D^H} \tag{40}$$

As depicted in Fig. 4, the hydrogen must first pass through the compressor before being sent to storage. The compressor consumes electricity, which varies according to the storage inputs:

$$P_t^{com} = K^c H_t^{in,sto} \quad \forall t \in \tau \tag{41}$$

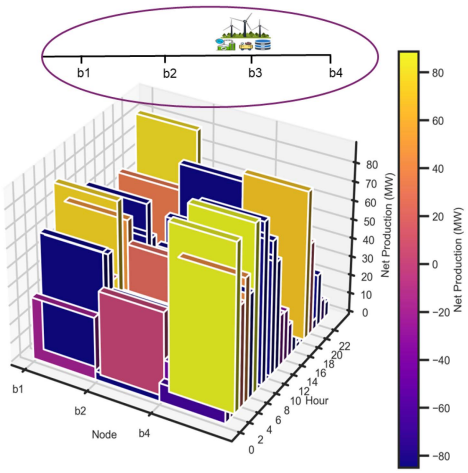

Fig. 5. Illustration of the 4 bus case study along with the hourly net production of the nodes.

The time-varying state of charge of the storage and its maximum allowable capacity are mathematically modeled in (42) and (43), respectively.

$$SOC_t^{sto} = SOC_{t-1}^{sto} + H_t^{in,sto} - H_t^{out,sto} \quad \forall t \in \tau \tag{42}$$

$$SOC_t^{sto} \leq \widehat{SOC^{sto}} \quad \forall t \in \tau \tag{43}$$

IV. Case Study I

The first case study presents a simplified model of the standard European High Voltage (HV) transmission network, using line parameters obtained from [29]. In Fig. 5, the network under consideration is illustrated, alongside the net production values for each node during the simulation. As the figure illustrates, the HSEW is located at bus $b3$ while other nodes include various types of generation units and demand. The timeslot is contemplated one hour. The hourly net production of other nodes is calculated by subtracting their hourly demand from their hourly production. Positive net production indicates that the

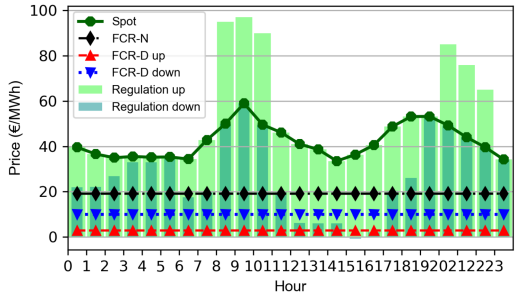

Fig. 6. Comparison of spot, FCRs, and regultaion prices on 1.4.2023 in Finland.

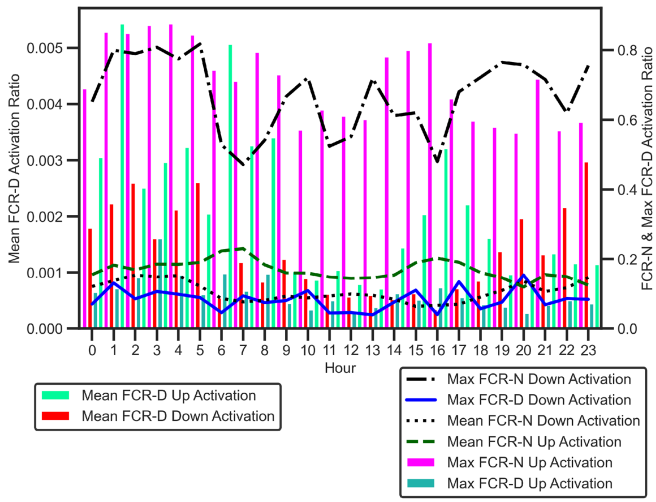

Fig. 7. The mean and maximum values of activation ratio estimated for the case study.

production exceeds the demand, while negative net production signifies higher demand than production. All specific details about the hydrogen electrolyzer, compressor and storage are sourced from [28]. The capacities are as follows: 52.25 MWh for the electrolyzer, 22 kg for hydrogen storage, and 42 MWh for the wind park. The daily demand for hydrogen is assumed to be 1222.44 kg.

This paper analyzes real-world price data from Finland on April 1, 2023. We focus on the annual capacity prices for three FCR markets: FCR-N, upward FCR-D, and downward FCR-D capacity markets. Fig. 6 illustrates a comparison of these prices.

This paper examines the activation ratios for FCRs by analyzing one-year historical frequency data from Finland, spanning from April 1, 2022, to March 31, 2023. The maximum frequency deviation values are determined using (7), (8), (13), and (14), while the mean frequency deviation values are estimated using (29)–(32). The activation ratios are computed by dividing the frequency deviations for FCR-N by 0.1 and those for FCR-D by 0.4, in order to account for their activation droop characteristics. Fig. 7 represents the estimated activation ratios for FCRs. For improved clarity in presentation, the mean values of FCR-D activation are depicted based on the left y-axis, while the remaining activation values are illustrated based on the right y-axis.

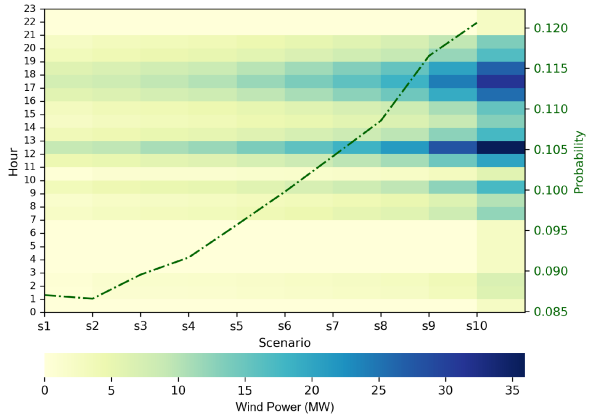

Fig. 8. The heatmap and line plots representing the wind power values and the probability for each scenario.

Furthermore, we consider six onshore wind turbines with full power converters, each with a capacity of 7 MWh, aligning with the 2020 ATB NREL turbine outlined in [30]. Essential turbine parameters and power curves can be referenced in the provided source. We utilized quantile regression to forecast wind power from forecasted wind speed, generated different scenarios from the quantiles and assign probability to each scenario using the CDF of the quantile [31]. Accordingly, 10 scenarios (s1-s10) are considered. In Fig. 8, the x-axis represents 10 scenarios labeled from s1 to s10. The left y-axis corresponds to the hour of the day, ranging from 0 to 23 hours. Each cell in the heatmap is colored according to the wind power values (in MW) for each scenario and hour, with lighter colors indicating lower wind power and darker colors indicating higher values. Additionally, there is a line plot overlaid on the heatmap. This line represents the probability associated with each scenario, as indicated on the right y-axis. For comparison purposes, this paper examines three different operation strategies. In all strategies, the HSEW plays a role in managing network congestion. However, their operation strategies differ as follows:

- *Proposed operation strategy:* The model suggested by this paper in which HSEW contributes to both FCR-N and FCR-D provision.
- *Spot strategy:* Introduced by [28] which optimizes HSEW operation based on spot market prices.
- *Self-sufficient strategy:* Designed to enhance Self-sufficiency. This model aims to minimize the power flowing into the local transmission network. The costs are also calculated based on spot market prices.

A. Simulation Results I

The optimization problem described by (1) through 43 has been formulated and solved using the JuMP package in Julia. Fig. 9 illustrates the optimized decision values, representing the FCR capacities to be offered in reserve markets. Given the paper's focus on addressing wind power uncertainties robustly, the proposed operation strategy with optimal scheduling prioritizes allocating more capacity to downward flexible capacities. Fig. 9

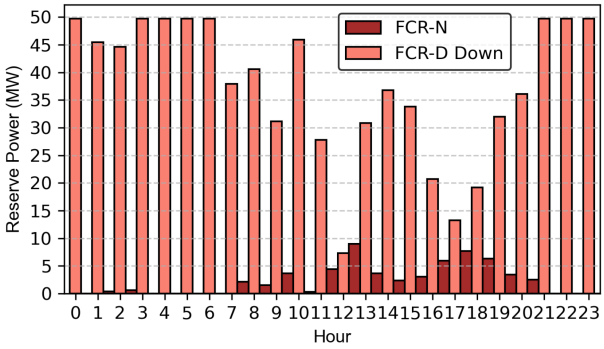

Fig. 9. Optimal capacities devoted to each reserve product in the proposed operation strategy.

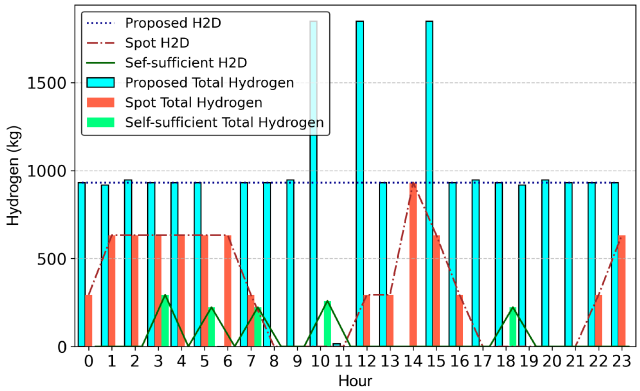

Fig. 10. Optimal hydrogen delivered to demand (H2D) and the total hydrogen produced by the electrolyzer (Total Hydrogen) for three studied strategies.

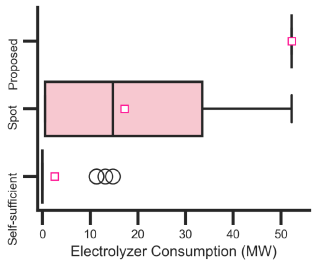

Fig. 11. The box plot representing the distribution of electrolyzer's consumption in three studied strategies.

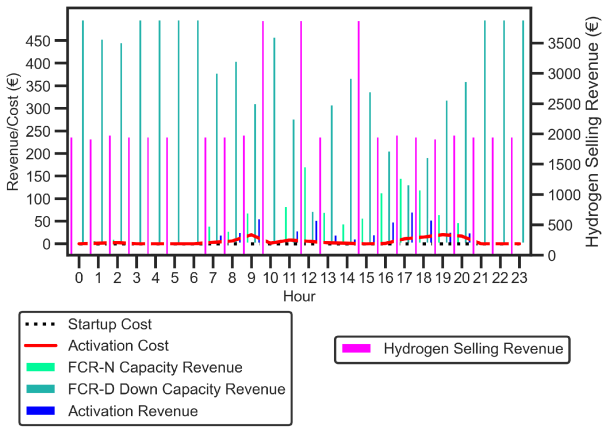

Fig. 12. The hourly illustration of costs and revenues brought from the proposed operation strategy.

showcases that the majority of HSEW capacity is allocated to downward FCR-D provision, with lesser capacity dedicated to symmetrical FCR-N provision, and none allocated to upward FCR-D capacity.

Furthermore, the Spot and Self-sufficient strategies were developed and solved using the JuMP package. Fig. 10 compares daily hydrogen production between these three strategies. "H2D" represents hydrogen delivered to meet demand, while "Total Hydrogen" signifies overall hydrogen production from the electrolyzer. The proposed operation strategy prioritizes hydrogen production alongside FCR market operations. Notably, it utilizes hydrogen storage and compression, leading to higher total hydrogen production compared to H2D at certain hours. In contrast, the Spot strategy follows spot market price patterns, with lower prices resulting in increased hydrogen production. The Spot strategy does not view hydrogen storage as a profitable option. Conversely, the Self-sufficient strategy minimizes hydrogen production to prevent excessive power entering the local grid. Hydrogen production occurs during hours of positive net production in the local transmission network. Similar to the Spot strategy, the Self-sufficient strategy does not utlize the storage. Fig. 11 further demonstrates that the proposed operation strategy maximizes the consumption of the electrolyzer, while the Spot strategy adjusts electrolyzer consumption according to spot prices. In contrast, the Self-sufficient strategy minimizes electrolyzer's electricity usage altogether. In this figure, the white square denotes the mean value of electrolyzer's consumption for each strategy.

Fig. 12 depicts the revenues and costs in the proposed operation strategy. Hydrogen selling revenue is shown on the right y-axis, while other costs and revenues are displayed on the left y-axis. The figure highlights that after hydrogen selling, a significant portion of HSEW revenue comes from FCR capacity revenue. Activation costs for downward FCR-N are relatively minor compared to its capacity revenue. Additionally, the optimized scheduling maintains the electrolyzer in ON-mode operation due to its high startup cost.

In contrast to the proposed operation strategy, the Self-sufficient and Spot strategies have limited revenue sources. HSEW profits solely from selling hydrogen and, if net production is positive, from selling wind power production at spot market prices. Conversely, when net production is negative, HSEW incurs costs for electricity consumption. Fig. 13 illustrates the costs and revenues when HSEW is optimized according to spot market prices. The figure reveals that buying electricity results in negative revenue when HSEW produces hydrogen. However, when hydrogen production ceases, HSEW can generate revenue by selling its wind production at spot market prices. Fig. 14 presents the revenues and costs associated with the Self-sufficient strategy. In this scenario, the electrolyzer is turned off for 5 hours, as the Self-sufficient strategy prioritizes

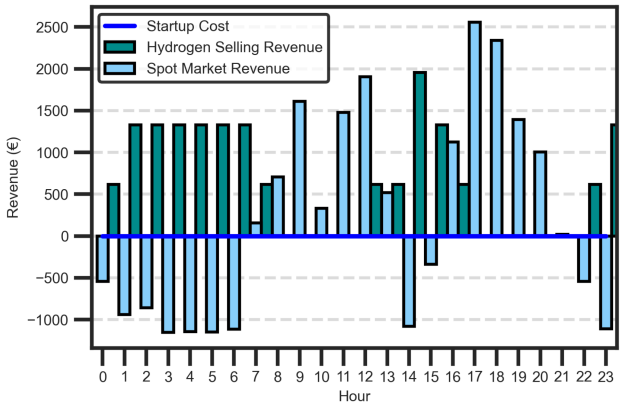

Fig. 13. The hourly illustration of costs and revenues brought from the spot-market-participation-based operation strategy.

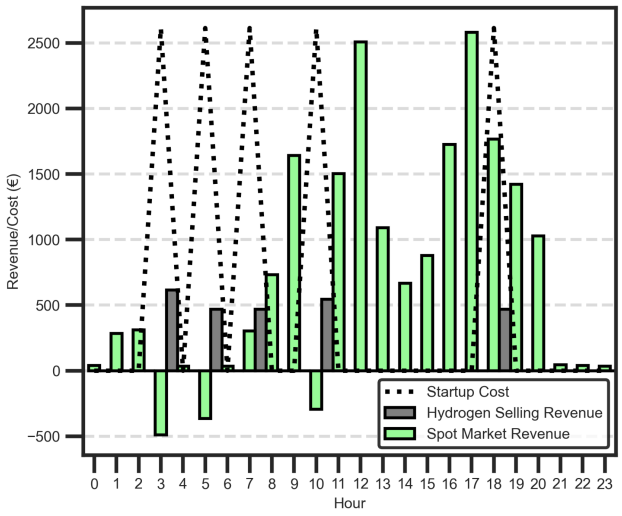

Fig. 14. The hourly illustration of costs and revenues brought for the Self-sufficient strategy.

TABLE II
COMPARISON OF TOTAL DAILY PROFIT FOR THREE STUDIED STRATEGIES

Strategies	Proposed	Spot	Self-sufficient
Profit (€)	57428.31	21440.37	7029.08

Self-sufficiency over economics. However, the high startup cost imposes significant expenses on HSEW in the Self-sufficient strategy.

Finally, Table II compares the daily profits obtained from these three strategies. The results show that participating in FCR markets can increase HSEW's profit by more than 2.6 times compared to when HSEW operates solely based on spot market prices. Additionally, the significant impact of startup costs is evident in the Self-sufficient strategy, where profits are 8 times lower than in the proposed operation strategy.

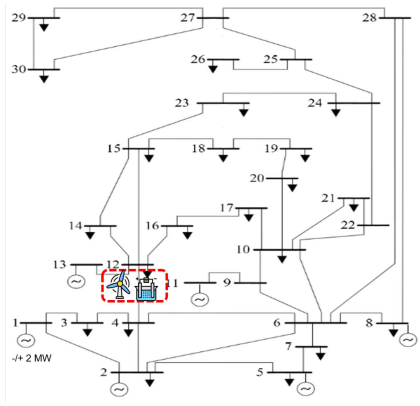

Fig. 15. The schematic of IEEE 30 bus system and the location of the HSEW in the network.

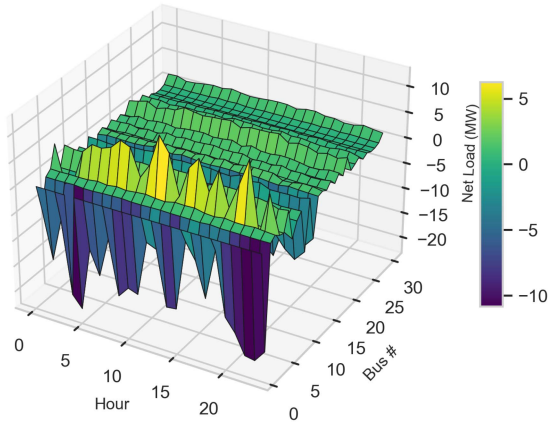

Fig. 16. Net demand (demand minus generation) values for buses in the IEEE 30-bus system.

V. CASE STUDY II

To demonstrate how the network affects HSEW's optimal operation, we place the HSEW within the IEEE 30-bus system [32]. Fig. 15 shows the network schematic, with the HSEW located at bus 12. Additionally, Fig. 16 illustrates the net demand (the difference between load and generation) within the network. Note that the HSEW maintains the same characteristics and specifications as in the first case study. The optimization problem is re-run using the IEEE 30-bus network setup.

A. Simulation Results II

Most reserve capacities are allocated to downward FCR-D, as the strategy aims to absorb excess wind generation, relying on minimum wind power forecasts. However, with the new network imposing additional constraints on HSEW operation, the optimal solution now includes less symmetrical reserve (FCR-N) and introduces upward FCR-D, unlike the 4-bus system, where no upward FCR-D was allocated. Fig. 17 shows the reserve allocations for the HSEW positioned at bus 12 in the IEEE 30-bus network.

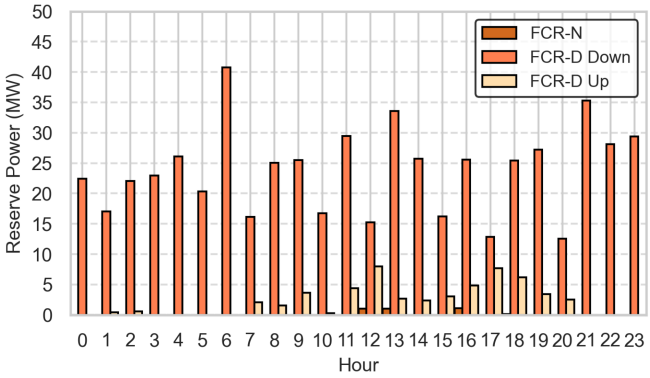

Fig. 17. Optimal capacities devoted to each reserve for the HSEW located in the IEEE 30-bus network.

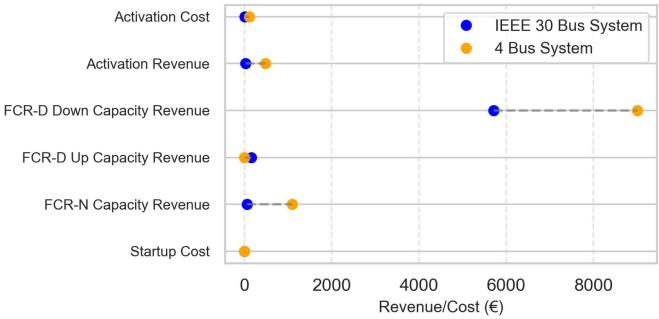

Fig. 18. Comparison of revenues and costs for the HSEW in the 4-bus network versus the IEEE 30-bus network.

Fig. 18 compares the revenues and costs of the HSEW in both the 4-bus and IEEE 30-bus networks. As shown, revenues from downward FCR-D decrease significantly due to the additional network-related constraints in the IEEE 30-bus network, which reduce flexibility for frequency-based services. A lower allocation to FCR-N is also observed in the IEEE 30-bus system, resulting in reduced activation costs and revenues for the HSEW. Similar to the 4-bus network, the HSEW in the 30-bus network incurs no startup costs, as the optimization consistently keeps the electrolyzer running without shutdowns.

In the HSEW simulation, the hydrogen storage starts with an initial state of charge (SOC) set at 0%. This initial SOC is then adjusted to 25%, 50%, 75%, and 100% to observe how the HSEW's optimal operations change with different starting levels. Interestingly, the reserved capacities remain the same across all four cases. The main difference is that as the SOC increases, more hydrogen is sold each hour, leading to higher revenue from hydrogen sales. Fig. 19 illustrates how the storage SOC changes over time in each scenario. As shown, the optimal strategy is to sell as much hydrogen as possible, fully depleting the storage, which allows for greater flexibility to offer downward FCRs. Table III compares revenues from hydrogen sales across scenarios with varying initial SOC levels. As anticipated, a higher initial SOC results in increased hydrogen sales revenue. However, the capacity allocated to reserves, and consequently, the revenue derived from them, remains constant across scenarios.

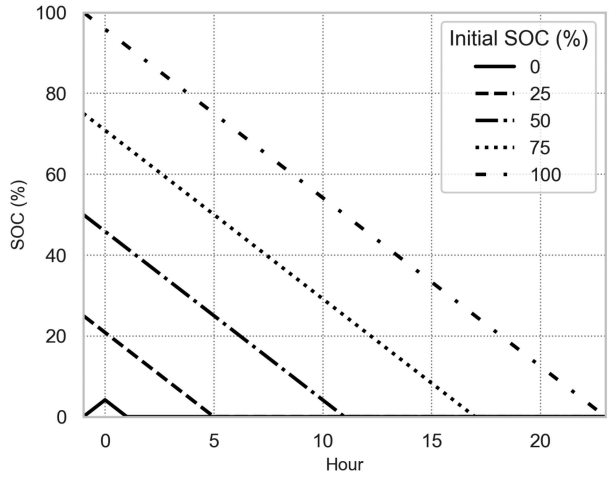

Fig. 19. Variation in hydrogen storage SOC during optimal HSEW operation for different initial SOC levels.

TABLE III
COMPARISON OF TOTAL DAILY REVENUE FROM HYDROGEN SALES

Initial SOC	0%	25%	50%	75%	100%
Revenue (€)	46969.1	58521.2	70073.2	81625.3	93177.4

VI. CONCLUSION

This paper introduced a novel method to optimize the coordination of HSEW operation to align with the requirements of the TSO. HSEW can serve multiple purposes, including providing FCR for normal operation and disturbance scenarios, as well as assisting with congestion management. The method addressed wind power uncertainty robustly while considering detailed electrolyzer states and FCR market characteristics, including activation features.

In the simulation section, we compared the performance and profitability of our proposed operation strategy with two others: Spot, which operates based on spot prices, and Self-sufficient, which emphasizes the grid's Self-sufficiency. The results showed that our proposed FCR-market-participation-based strategy produces significantly more hydrogen compared to the other strategies whereas the Self-sufficient operation strategy minimizes hydrogen production. Also, utilizing the hydrogen storage was only found to be profitable in the proposed operation strategy. In profitability, our FCR participation strategy earns 2.6 times more than the Spot-market-participation-based operation strategy and 8 times more than the Self-sufficient one.

In future, this paper can be extended in following directions:

- Since this paper focuses on the day-ahead scheduling, the real-time operation of an alkaline electrolyzer can be enhanced by using a detailed model that considers the effects of operational temperature and heat release. Understanding how these factors influence the electrolyzer's response to frequency changes in the power grid is essential. Future research can focus on optimizing temperature and pressure settings, as well as managing current density, to improve the electrolyzer's performance in real-time operations.

- A comprehensive future study is needed to assess the impact of different electrolyzer operations on spot prices. This research could be conducted across various systems with diverse generation mixes and consumption behaviors.

REFERENCES

[1] A. Iliceto, N. Samovich, N. Sousa e Silva, and A. Ilo, "Hydrogen's impact on grids: Impact of hydrogen integration on power grids and energy systems," Pub. Office Eur. Union, Tech. Rep. MJ-07-23-308-EN-N, 2023.

[2] O. Ruhnau, "How flexible electricity demand stabilizes wind and solar market values: The case of hydrogen electrolyzers," *Appl. Energy*, vol. 307, 2022, Art. no. 118194. [Online]. Available: https://www.sciencedirect.com/science/article/pii/S0306261921014641

[3] C. Zhang et al., "Flexible grid-based electrolysis hydrogen production for fuel cell vehicles reduces costs and greenhouse gas emissions," *Appl. Energy*, vol. 278, 2020, Art. no. 115651. [Online]. Available: https://www.sciencedirect.com/science/article/pii/S0306261920311491

[4] G. Longoria, M. Lynch, and J. Curtis, "Green hydrogen for heating and its impact on the power system," *Int. J. Hydrogen Energy*, vol. 46, no. 53, pp. 26725–26740, 2021.

[5] C. Feng, C. Shao, Y. Xiao, Z. Dong, and X. Wang, "Day-ahead strategic operation of hydrogen energy service providers," *IEEE Trans. Smart Grid*, vol. 13, no. 5, pp. 3493–3507, Sep. 2022.

[6] W. Zhang, A. Maleki, and M. Alhuyi Nazari, "Optimal operation of a hydrogen station using multi-source renewable energy (solar/wind) by a new approach," *J. Energy Storage*, vol. 53, 2022, Art. no. 104983. [Online]. Available: https://www.sciencedirect.com/science/article/pii/S2352152X22009884

[7] F. Alshehri, V. G. Suárez, J. L. Rueda Torres, A. Perilla, and M. van der Meijden, "Modelling and evaluation of PEM hydrogen technologies for frequency ancillary services in future multi-energy sustainable power systems," *Heliyon*, vol. 5, no. 4, 2019, Art. no. e01396. [Online]. Available: https://www.sciencedirect.com/science/article/pii/S2405844018367471

[8] C. Huang, Y. Zong, S. You, and C. Træholt, "Analytical modeling and control of grid-scale alkaline electrolyzer plant for frequency support in wind-dominated electricity-hydrogen systems," *IEEE Trans. Sustain. Energy*, vol. 14, no. 1, pp. 217–232, Jan. 2023.

[9] S. Mucci, A. Mitsos, and D. Bongartz, "Power-to-x processes based on PEM water electrolyzers: A review of process integration and flexible operation," *Comput. Chem. Eng.*, vol. 175, 2023, Art. no. 108260. [Online]. Available: https://www.sciencedirect.com/science/article/pii/S0098135423001308

[10] M. B. Hossain, M. R. Islam, K. M. Muttaqi, D. Sutanto, and A. P. Agalgaonkar, "Power system dynamic performance analysis based on frequency control by proton exchange membrane electrolyzers," *IEEE Trans. Ind. Appl.*, vol. 59, no. 4, pp. 4998–5008, Jul./Aug. 2023.

[11] M. Ghazavi Dozein, A. Maria De Corato, and P. Mancarella, "Fast frequency response provision from large-scale hydrogen electrolyzers considering stack voltage-current nonlinearity," in *Proc. 2021 IEEE Madrid PowerTech*, 2021, pp. 1–6.

[12] M. G. Dozein, A. Jalali, and P. Mancarella, "Fast frequency response from utility-scale hydrogen electrolyzers," *IEEE Trans. Sustain. Energy*, vol. 12, no. 3, pp. 1707–1717, Jul. 2021.

[13] A. M. De Corato, S. Riaz, and P. Mancarella, "Impact of hydrogen electrolyzers on flexibility and network voltage profiles of a virtual power plant," in *Proc. 2020 Australas. Universities Power Eng. Conf.*, 2020, pp. 1–6.

[14] N. Veerakumar et al., "Fast active power-frequency support methods by large scale electrolyzers for multi-energy systems," in *Proc. 2020 IEEE PES Innov. Smart Grid Technol. Eur.*. IEEE, 2020, pp. 151–155.

[15] M. G. Dozein, A. M. De Corato, and P. Mancarella, "Virtual inertia response and frequency control ancillary services from hydrogen electrolyzers," *IEEE Trans. Power Syst.*, vol. 38, no. 3, pp. 2447–2459, May 2023.

[16] I. Pavić, N. Čović, and H. Pandžić, "PV–battery-hydrogen plant: Cutting green hydrogen costs through multi-market positioning," *Appl. Energy*, vol. 328, 2022, Art. no. 120103. [Online]. Available: https://www.sciencedirect.com/science/article/pii/S0306261922013605

[17] M. Maluenda, S. Cordova, A. Lorca, and M. Negrete-Pincetic, "Optimal operation scheduling of a PV-Bess-Electrolyzer system for hydrogen production and frequency regulation," *Appl. Energy*, vol. 344, 2023, Art. no. 121243.

[18] M. Agredano-Torres, M. Zhang, L. Söder, and Q. Xu, "Decentralized dynamic power sharing control for frequency regulation using hybrid hydrogen electrolyzer systems," *IEEE Trans. Sustain. Energy*, vol. 15, no. 3, pp. 1847–1858, Jul. 2024.

[19] E. Crespi, P. Colbertaldo, G. Guandalini, and S. Campanari, "Energy storage with power-to-power systems relying on photovoltaic and hydrogen: Modelling the operation with secondary reserve provision," *J. Energy Storage*, vol. 55, 2022, Art. no. 105613. [Online]. Available: https://www.sciencedirect.com/science/article/pii/S2352152X22016012

[20] A. Lüth, Y. Werner, R. Egging-Bratseth, and J. Kazempour, "Electrolysis as a flexibility resource on energy islands: The case of the north sea," *Energy Policy*, vol. 185, 2024, Art. no. 113921.

[21] X. Cheng et al., "A coordinated frequency regulation and bidding method for wind-electrolysis joint systems participating within ancillary services markets," *IEEE Trans. Sustain. Energy*, vol. 14, no. 3, pp. 1370–1384, Jul. 2023.

[22] M. Saretta, E. Raheli, and J. Kazempour, "Electrolyzer scheduling for nordic FCR services," in *Proc. 2023 IEEE Int. Conf. Communications, Control, Comput. Technol. Smart Grids*, 2023, pp. 1–6.

[23] "FCR-design project summary report by ENTSO-E," 2019. [Online]. Available: https://www.statnett.no/globalassets/for-aktorer-i-kraftsystemet/utvikling-av-kraftsystemet/nordisk-frekvensstabilitet/fcr-design-project-summary-report.pdf

[24] M. Sánchez, E. Amores, L. Rodríguez, and C. Clemente-Jul, "Semi-empirical model and experimental validation for the performance evaluation of a 15 kW alkaline water electrolyzer," *Int. J. Hydrogen Energy*, vol. 43, no. 45, pp. 20332–20345, 2018.

[25] C. Varela, M. Mostafa, and E. Zondervan, "Modeling alkaline water electrolysis for power-to-x applications: A scheduling approach," *Int. J. Hydrogen Energy*, vol. 46, no. 14, pp. 9303–9313, 2021.

[26] H. Khajeh, C. Parthasarathy, E. Doroudchi, and H. Laaksonen, "Optimized siting and sizing of distribution-network-connected battery energy storage system providing flexibility services for system operators," *Energy*, vol. 285, 2023, Art. no. 129490.

[27] "Terms and conditions for providers of frequency containment reserves (FCR) by Fingrid," 2023. [Online]. Available: https://www.fingrid.fi/globalassets/dokumentit/fi/sahkomarkkinat/reservit/terms-and-conditions-for-providers-of-frequency-containment-reserves-fcr-as-of-22-may-2023.pdf

[28] M. T. Baumhof, E. Raheli, A. G. Johnsen, and J. Kazempour, "Optimization of hybrid power plants: When is a detailed electrolyzer model necessary?," in *Proc. 2023 IEEE Belgrade PowerTech*, 2023, pp. 1–10.

[29] CIGRE, "Benchmark systems for network integration of renewable and distributed energy resources," 2014. [Online]. Available: https://www.e-cigre.org/publications/detail/575-benchmark-systems-for-network-integration-of-renewable-and-distributed-energy-resources.html

[30] NREL, "2020ATB NREL reference 7MW 200," 2020. [Online]. Available: https://nrel.github.io/turbine-models/2020ATB_NREL_Reference_7MW_200.html

[31] D. Burba, "Probabilistic ML with quantile matching: An example with Python," 2023. [Online]. Available: https://towardsdatascience.com/probabilistic-ml-with-quantile-matching-an-example-with-python-c367eee 85f 18

[32] University of Washington Power Systems Test Case Archive, "Power flow test case: 30 bus system," 1993. Accessed: Nov. 07, 2024. [Online]. Available: https://labs.ece.uw.edu/pstca/pf30/pg_tca30bus.htm